Hot Forward-Extruded Nanocrystalline Anisotropic Nd-Fe-B Magnetic Sheets with High Magnetic Properties

LIYUN ZHENG [1,2,5] LIN YUE,[2] LIU SU,[3] MINGGANG ZHU,[1] YIKUN FANG,[1] LIXIN ZHAO,[2,4,6] LICHENG WU,[2] and WEI LI[1,7]

1.—Research Institute of Functional Materials, Central Iron and Steel Research Institute Co., Ltd., Beijing 100081, China. 2.—Hebei Engineering Research Centre for Rare Earth Permanent Magnetic Materials and Applications, Hebei University of Engineering, Handan 056038, Hebei, China. 3.—Institute of Scientific and Technical Information of Handan, Handan 056038, Hebei, China. 4.—School of Mechanical and Equipment Engineering, Hebei University of Engineering, Handan 056038, Hebei, China. 5.—e-mail: zhengliyun@126.com. 6.—e-mail: zhaolx1120@126.com. 7.—e-mail: wwweili@126.com

Anisotropic Nd-Fe-B magnets have been fabricated by the hot forward-extrusion method and exhibit the same heterogeneous microstructure characteristics as conventional die-upsetting magnets. It has been found that the magnetic properties on both sides of the magnetic sheet are better than that of the middle zone, and that the magnetic properties of the intermediate zone in the extrusion direction are better than those of the top zone (close to the extrusion die and the latest extruded zone) and the bottom zone (the earliest extruded zone) in the extrusion direction. With the decrease of extrusion speed, the process by which $Nd_2Fe_{14}B$ grains become flat platelets with their c-axes parallel to the stress axis by grain rotating and diffusion slip have been more fully completed, while the texture, remanence, and maximum magnetic energy product $(BH)_{max}$ of the forward-extruded magnetic sheet monotonically increased. With the increase of hot-pressing and hot-extrusion temperatures, the texture, remanence, and $(BH)_{max}$ of the hot-extruded magnetic sheet initially increased and then decreased. The magnetic sheet hot-pressed at 550°C and hot-extruded at 850°C with an extrusion speed of 0.05 mm s^{-1} had the best magnetic properties, its $(BH)_{max}$ being 40.3 MGOe, B_r 13.5 kGs, and H_{cj} 9.8 kOe.

INTRODUCTION

Nd-Fe-B rare-earth permanent magnetic material since its invention in 1984 is listed as the third generation of rare-earth permanent magnetic materials,[1,2] known as the "magnetic king" due to its high remanence, high coercivity, and high maximum magnetic energy product.[3] After nearly 40 years' development, it has been widely used in new energy cars, energy-efficient appliances, consumer electronics, industrial motors, wind power, and other fields.[4,5] Hot pressing and hot deformation is an important forming technique for

anisotropic Nd-Fe-B magnets,[6–8] which has the characteristics of simple process and short forming time, obtaining excellent crystal orientation without a magnetic field. During the hot-pressing process, the Nd-Fe-B melt-spun powders are pressed to obtain a full-density isotropic Nd-Fe-B semi-finished product, which is then deformed or extruded. During the hot-deformation process, $Nd_2Fe_{14}B$ grains diffuse and precipitate parallel to the pressure direction, forming an anisotropic magnet with a c-axis texture.

There are three hot-deformation methods for Nd-Fe-B magnets, die upsetting, reverse or backward extrusion, and forward extrusion. Die upsetting is mainly used for the sheet production of Nd-Fe-B magnets, and laboratory samples have reached

50.2 MGOe.[9] However, the magnetic properties of the die-upsetting Nd-Fe-B magnet are not uniform in the plane perpendicular to the pressure direction, and decrease from the center to the edge due to its uneven deformation. In 1987, Daido applied for a patent for the preparation of radial magnetic rings by the reverse-extrusion method.[10] After more than 20 years research and development, the magnetic ring products of Daido Steel have reached a magnetic energy product of 44 MGOe and a coercivity of 21.5 kOe. The preparation of Nd-Fe-B magnetic rings by backward extrusion has the advantages of good radiation orientation and uniform magnetic performance. However, the length of the backward-extruded Nd-Fe-B magnet is limited. A forward-extruded Nd-Fe-B magnet can obtain longer length and more uniformity in the length direction and has less material loss than the backward-extruded Nd-Fe-B magnet, and recently attracting more attentions.

Li et al.[11] prepared a flake Nd-Fe-B magnet with a magnetic energy product of 30.3 MGOe by pressing at room temperature instead of hot pressing and positive extrusion. Their results demonstrate that a positive-extrusion magnet has the same microstructure as magnets using the die-forging upsetting rough and reverse extrusion methods, and shows a heterogeneous microstructure consisting of coarse grain and fine grain regions, and has been widely reported.[11–13] This method is of great significance for mass production and the forming of magnets of other shapes. However, normal atmospheric temperature pressing instead of hot pressing causes loss of magnetic properties, which has a certain gap compared with backward extrusion. Therefore, the aim of this work is to tune the process of forward extrusion to improve the structures and properties of hot forward-extruded magnetic sheets and to explore the forming mechanism of the sheets.

EXPERIMENTAL

A set of new forward-extrusion molds for magnetic sheets were designed, including two steps of hot pressing and hot deformation, as shown in Fig. 1a before and after hot pressing, and Fig. 1b before and after hot deformation. The deformation part adopts a "funnel" excess (shown in Fig. 1b and c), to ensure that the grains form a texture along the long side during the hot deformation process, thereby avoiding the formation of a planar texture at the equiaxial extrusion port,[14] and reducing friction to diminish the occurrence of cracks. The deformed part was placed in the cavity of the support cylinder without contact with the mold, avoiding the step of demolding and its damage to the product, decreasing the contact with the mold for too long a time, thereby reducing the influence of high temperature on the magnetic properties.

The commercial magnetic powders, MQU-F, from Magnequench (Tianjin) with a nominal composition of $Nd_{29.1}Pr_{0.2}Fe_{63.66}Co_{5.5}Ga_{0.5}Dy_{0.01}B_{0.87}$ were used as the initial material for preparing Nd-Fe-B
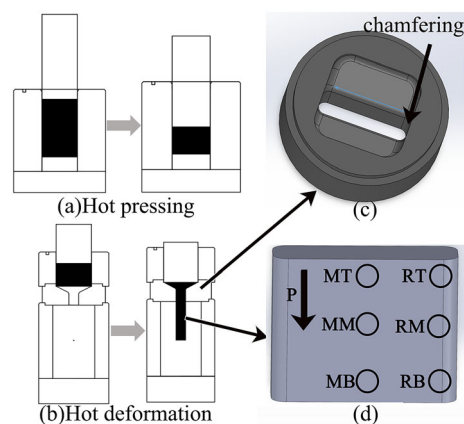

Fig. 1. Schematics of hot forward-extrusion molds for (a) hot pressing, (b) hot deformation, (c) 3D stereogram of the extrusion die, and (d) the top-right (RT), top-middle (MT), center (MM), middle-right (RM), bottom-middle (MB), bottom-right (RB) samples' position (the arrow P indicates the extrusion direction or press direction).

magnetic rings. In our previous work, the composite-extruded Nd-Fe-B magnetic rings with the same composition hot-pressed at 550°C for 1 min and hot-extruded at 850°C using a deformation rate of 0.15 mm s^{-1} obtained $(BH)_{max}$, B_r, H_{cj} values of 38.52 MGOe, 13.35 kGs, and 11.65 kOe, respectively.[15] Thus, the magnetic powders were hot-pressed under 150 MPa in vacuum at 500–600°C for 1 min to obtain a blank and then forward-extruded under approximately 150 MPa at 800–900°C to finish the extrusion process (about 2 min). The remanence and energy product of the hot-deformed Nd-Fe-B magnet both rise with the decrease of the strain rate.[16] So, we selected the range of deformation rate of 0.03–0.07 mm s^{-1}, and Nd-Fe-B magnetic sheets were prepared. To quantify the deformation level, the cross-section shrinkage rate, ε_A, was calculated according to $\varepsilon_A = (A_0 - A_1)/A_0 \times 100\%$, in which A_0 and A_1 are the cross-section areas of the blank before and after extrusion deformation, respectively. In this work, the hot-pressed blank has a width, thickness, and length of 25 mm, 25 mm, and 18 mm, the extruded magnet has a width, thickness, and length of 25 mm, 7 mm, and 30 mm, respectively, thus the cross-section shrinkage rates were the same as 72%.

Due to the symmetrical structure of the magnetic sheet, the six samples located in the top-right (RT), top-middle (MT), center (MM), middle-right (RM), bottom-middle (MB), and bottom-right (RB) of the magnetic sheet shown in Fig. 1c were cut, tested, and analyzed. The cylinder samples with a diameter of 6 mm after grinding and polishing were used to test the magnetic properties along the radial direction by a NIM-6200C hysteresisgraph meter after previous saturation with a pulse magnetizer at 100 kOe. Square samples with a size of 5×5 mm^2 were tested by X-ray diffraction (XRD; Ultima IV; Rigaku) using Cu Kα radiation and a scanning

Table I. Magnetic properties and $I_{(006)}/I_{(105)}$ ratios of the samples for different positions of the magnetic sheet hot-pressed at 550°C and forward-extruded at 800°C with the deformation speed of 0.05 mm s^{-1}

Sample position	B_r (Gs)	H_{cj} (kOe)	$(BH)_{max}$ (MGOe)	$I_{(006)}/I_{(105)}$
RT	10.08	11.07	20.98	0.42
RM	13.66	9.06	39.65	1.17
RB	12.29	10.65	31.11	0.56
MT	8.77	11.57	13.46	0.34
MM	11.71	10.36	31.58	0.78
MB	11.95	10.25	25.06	0.48
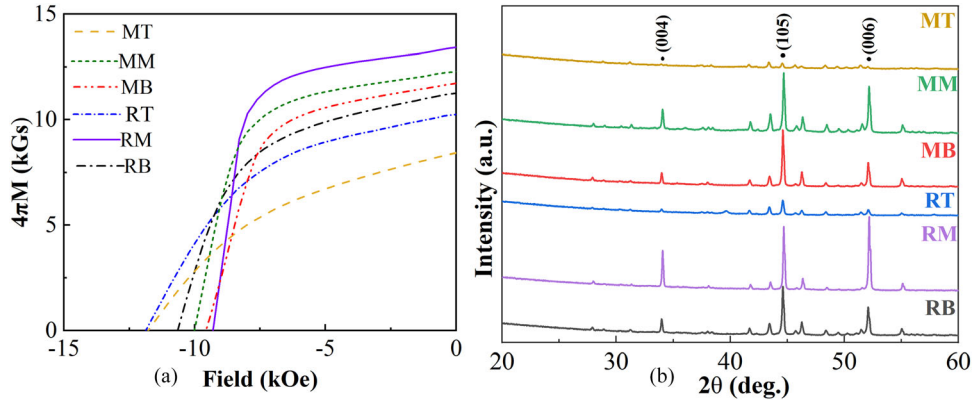
Fig. 2. (a) Demagnetization curves and (b) XRD patterns of the 6 samples of the magnetic sheet hot-pressed at 550°C and forward-extruded at 800°C with the deformation speed of 0.05 mm s^{-1}.

electron microscope (SEM; JSM-7001F; JEOL) to analyze the phase structure and microstructure of the magnetic sheets.

RESULTS AND DISCUSSION

Table I and Fig. 2a and b show the magnetic properties, $I_{(006)}/I_{(105)}$, demagnetization curve, and XRD patterns of the RT, RM, RB, MT, MM, and MB samples of the magnetic sheet hot-pressed at 550°C and forward-extruded at 800°C with deformation speed of 0.05 mm s^{-1}. It can be seen that the maximum magnetic energy products, $(BH)_{max}$, and remanences of the RT, RM, and RB samples located in the edges and sides are higher than those of the corresponding MT, MM, and MB samples in the center, respectively. For the samples in the right edge, the $(BH)_{max}$ of the central RM sample is higher than those of the RT and RB samples in the top and bottom zones. For the samples in the central column, the MM sample has a higher $(BH)_{max}$ than the MF and MB samples. From Table I, it can also be seen that the remanences increased with the increase of texture degree (shown in Figure S-1 in the Supplementary material).

Magnetic anisotropy is formed during deformation. Equiaxed grains are transformed into sheet grains, which are oriented in the direction of pressure to form a texture, which is conducive to the magnetic properties of the material.[17] There are chamfers with radius 2 mm on both sides of the mold deformation port (Fig. 1c), so that the thickness of both sides is smaller than that of the middle part. Li et al.[11] found that the smaller the extrusion thickness, the better its magnetic properties. The smaller the thickness, the amount of deformation also increases, so the texture is better, and the magnetic properties of both side edges are better than the middle. From Fig. 2b and Table I, it can be seen that the intensity ratio of the (006) and (105) diffraction peak of the RM sample, $I_{(006)}/I_{(105)}$, is 1.169 and higher than that of the MM sample, 0.78, indicating that the texture of the RM sample is better than that of the MM sample. From Fig. 2b and Table I, it can also be seen that the intensities of the (006) and (105) peaks of the RB sample are significantly stronger than those of the RT and RB samples, and the $I_{(006)}/I_{(105)}$ of the RM sample is 1.17 and higher than that of the RT and RB samples, indicating a stronger c-axis texture. The (105) and (006) peaks of the RT sample are extremely low and the $I_{(006)}/I_{(105)}$ of the RT sample is 0.42 and lower than that of the RB sample, indicating a weaker texture than the RB sample.

Figure 3 shows the cross-section morphologies of the RM (Fig. 3a and b) and MM (Fig. 3c and d) samples of the magnetic sheet hot-pressed at 550°C and forward-extruded at 800°C with the deformation speed of 0.05 mm s^{-1}. From Fig. 3a and c, it can be seen that the magnetic sheet RM (Fig. 3a and b) coarse grain area, and the fine grain area are almost
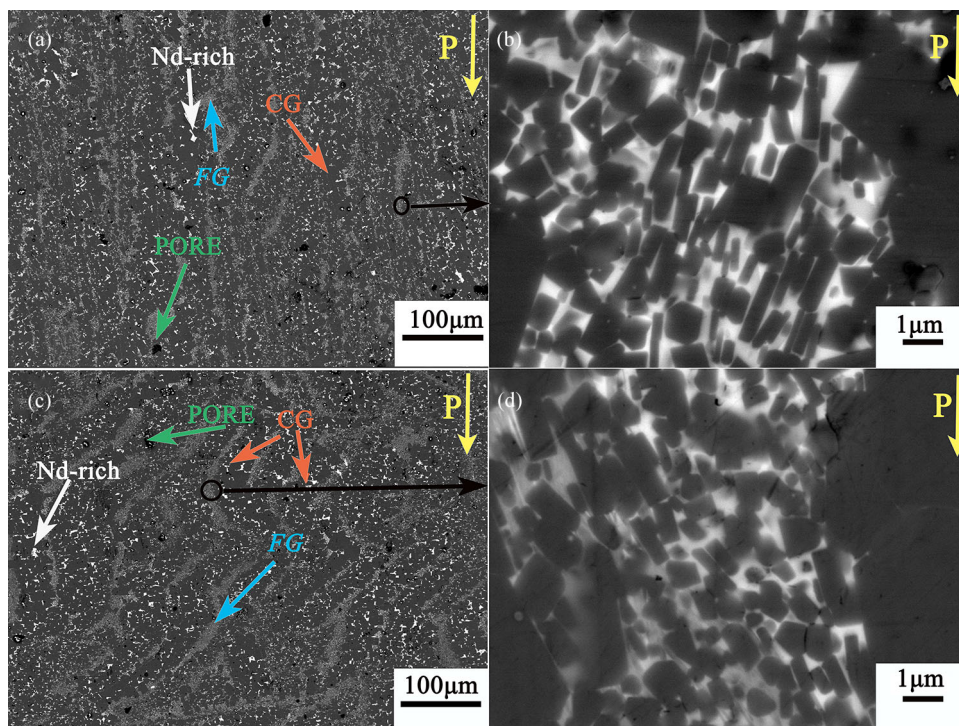
Fig. 3. Cross-section morphologies of (a, b) the RM samples and (c, d) the MM samples of the magnetic sheet hot-pressed at 550°C and forward-extruded at 800°C with the deformation speed of 0.05 mm s^{-1}. *CG* coarse grains, *FG* fine grains.

parallel to the pressure direction, while the MM (Fig. 3c and d) has an arc distribution. The RM sample's proximity to the edge is a little bit thinner due to a chamfering design of 2 mm in the extrusion port. Thus, the stress proximity to the edge is a little bit higher under the same force during the extrusion process and the amount of deformation also increases, which is more conducive to the formation of texture and prevents the emergence of non-pressure direction sheet tissue. Thus, the RM sample has a higher remanence than the MM sample. All the fine grain areas of the RM (Fig. 3a and b) sample are almost lamellar grains, while the MM sample still has partly spherical or polygonal grains. The average length and width of lamellar grains of the RM (Fig. 3a and b) sample are 1.44 μm and 0.37 μm, respectively (shown in Table S-1 in the Supplementary material), while those of the MM (Fig. 3c and d) sample are 1.25 μm and 0.39 μm, respectively (shown in Table S-1 in the Supplementary material). Therefore, the magnetic properties of the RM samples on both sides of the magnetic sheet are better than those of the samples in the middle, which also confirms the results of XRD.

To further understand the formation mechanism of the texture and the reasons for the difference of the magnetic properties during hot deformation, Fig. 4 shows a schematic of the texture-forming mechanism and the cross-section morphologies of RT (Fig. 4b and c), RM (Fig. 4d and e), and RB (Fig. 4f and g) samples of the magnetic sheet hot-pressed at 550°C and forward-extruded at 800°C

with the deformation speed of 0.05 mm s^{-1}. In the early stage of deformation, the stress is smaller and the sample has better fluidity; thus, a small number of short flaky grains with larger thickness and smaller length and spherical grains were formed (Fig. 4g). However, the angle between the grain orientation direction and the pressure direction was large, and there were more fine pores (Fig. 4f). The texture and compactness of the RB (Fig. 4f and g) sample were poor, resulting in the lower remanence and $(BH)_{max}$ of the RB (Fig. 4f and g) sample. With the progress of deformation, the remaining time at a high temperature of the blank became longer, the grain size increased, and the deformation resistance gradually increased. Almost all the grains were transformed into slender lamellar grains, and grew parallel along the pressure, forming a good texture. The flow rate became slower and the deformation more fully uniform. The grains of the RM (Fig. 4d and e) sample in the middle sheet became more slender and there were fewer pores. The remanence and $(BH)_{max}$ of the RM (Fig. 4d and e) sample reached the highest. In the later stage of deformation, the undeformed part of the blank experienced a long time at high temperature, and the grains grew before deformation and became more difficult to deform into platelet grains. From Fig. 4c, we can see that most of the grains of the RT (Fig. 4b and c) sample are still spherical, which is related to the small amount of initial deformation, resulting in a significant decline of the remanence of the RT (Fig. 4b and c) sample. This is consistent with the
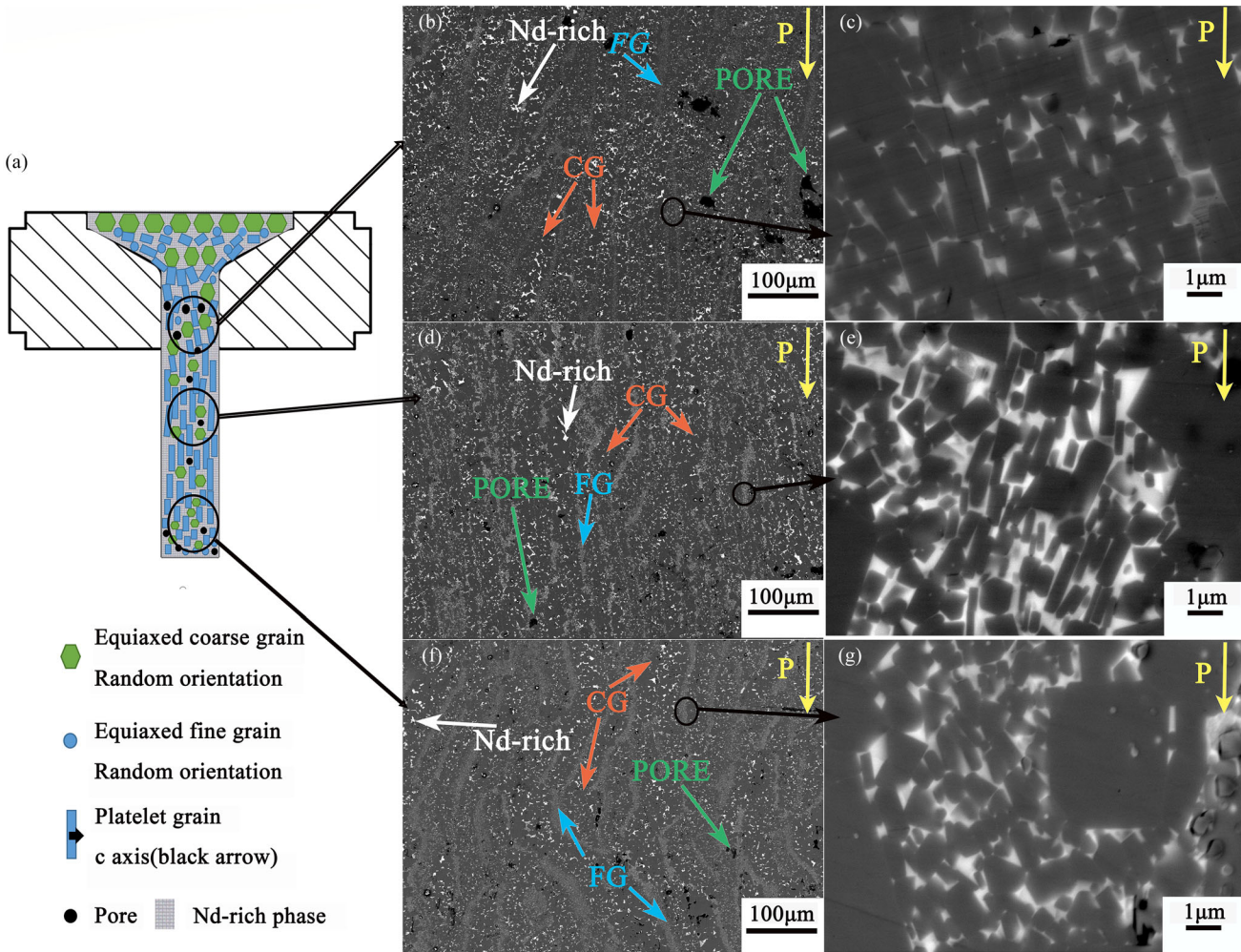
Fig. 4. (a) Schematic of the texture-forming mechanism and the cross-section morphologies of (b, c) RT, (d, e) RM, and (f, g) RB samples of the magnetic sheet hot-pressed at 550°C and forward-extruded at 800°C with the deformation speed of 0.05 mm s^{-1}.

XRD analysis. The coarse grains and a large number of Nd-rich phase aggregation appear, the mold-release agent reduces and deformation resistance become greater, resulting in deeper cracks, and many pores in the RT (Fig. 4b and c) sample located in the upper part of the magnetic sheet (Fig. 4b). These cracks and pores lead to a significant decline in magnetic properties. The RM (Fig. 3a and b) and MM (Fig. 3c and d) samples have similar microstructures because these two samples are located at the same extrusion height. The microstructures of the RT (Fig. 4b and c), RM (Fig. 4d and e) and RB (Fig. 4f and g) samples show large changes, because these samples are located at different extrusion heights. The RT sample locates in the top zone of the extruded magnetic sheet, the closest position to the extrusion die, which means that the sample has not been fully finished in orientation very well and does not shown a parallel-arranged heterogeneous microstructure. The RB (Fig. 4f and g) sample is located in the bottom zone of the extruded magnetic sheet, which is extruded

the earliest and the bottom end is not under force. Thus, the microstructure of this sample is a little bit different to that of the RM (Fig. 4d and e) sample.

To investigate the influence of the hot-pressing temperature on the forward-extruded magnetic sheet, the MM samples of the magnetic sheets hot-pressed at different temperatures and forward-extruded at 800°C with the deformation speed of 0.05 mm s^{-1} were cut and characterized. Figure 5 shows the demagnetization curves and XRD patterns, and Table II shows the magnetic properties and $I_{(006)}/I_{(105)}$ of these MM samples.

As can be seen from Fig. 5a and Table II, the remanences and $(BH)_{max}$ initially increase with the hot-pressing temperatures and then decrease. The sample hot-pressed at 550°C has the highest remanence and $(BH)_{max}$, 11.71 kGs and 31.58 MGOe, respectively. The hot-pressing temperature affects the grain size, compactness, and plastic deformation ability of the compact blank, which in turn affects the formation of the texture of the hot-deformed magnet.
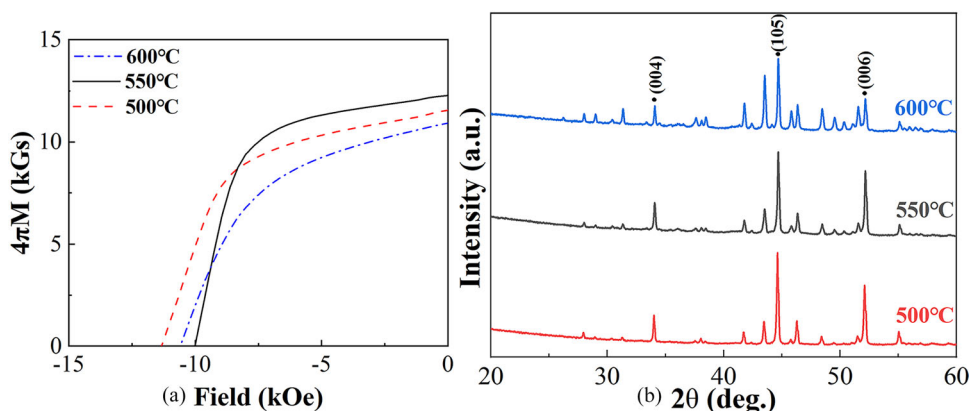
Fig. 5. (a) Demagnetization curves and (b) XRD patterns of the MM samples from the magnetic sheet hot-pressed at different hot-pressing temperatures and forward-extruded at 800°C with the deformation speed of 0.05 mm s^{-1}.

Table II. The magnetic properties and $I_{(006)}/I_{(105)}$ of the MM samples from the magnetic sheet fabricated under different processes

Hot pressing temperature (°C)	Deformation speed (mm s^{-1})	Deformation temperature (°C)	B_r (Gs)	H_{cj} (kOe)	$(BH)_{max}$ (MGOe)	$I_{(006)}/I_{(105)}$
500	0.05	800	11.38	10.64	26.83	0.64
550	0.05	800	11.71	10.36	31.58	0.78
600	0.05	800	10.8	10.08	22.66	0.43
550	0.03	800	13.30	9.97	37.84	1.09
550	0.05	800	11.71	10.36	31.58	0.78
550	0.07	800	9.61	10.93	18.13	0.57
550	0.05	800	11.71	10.36	31.58	0.78
550	0.05	850	13.58	10.40	40.29	1.28
550	0.05	900	6.42	12.24	8.35	0.32

From Fig. 5b and Table II, it can be seen that the $I_{(006)}/I_{(105)}$ values of the samples hot-pressed at 500°C, 550°C, and 600°C are 0.64, 0.78, and 0.43, respectively. The sample hot-pressed at 550°C has the highest $I_{(006)}/I_{(105)}$, indicating the best texture and orientation. This is because the blank hot-pressed at 550°C obtains a high density, preventing the appearance of coarse grains, and has better plasticity, which is more conducive to the formation of textures during the subsequent hot deformation, and thus better magnetic properties.

Figure 6 shows the cross-section morphologies of the MM samples from the magnetic sheets hot-pressed at different temperature and forward-extruded at 800°C with the deformation speed of 0.05 mm s^{-1}. From Fig. 6, it can be seen that the hot-deformed grains are gradually growing with the increase of hot-pressing temperature. Because the hot-deformation process is uniaxial deformation, the finer grains are transformed from spherical to platelet after deformation. The development mechanism of this texture has been discussed in Ref. 17. In contrast, it is difficult to change the shape of the coarser grains. As shown in Fig. 6f, most of the grains in the sample hot-pressed at 600°C are coarse equiaxed crystals, which rarely transform

into platelet crystals and cannot form a good texture. The remanence and coercivity of the sample are relatively low, resulting in a very low magnetic energy product.

From Table II, it can be seen that the sample hot-pressed at 500°C has the lowest density. The rare-earth-rich phase in the grain boundary has not reached the temperature of plastic deformation, and the plasticity of the blank is poor.[18] There are fewer spherical grains that transform into lamellar grains during the subsequent hot-deformation process, thus leading to lower magnetic properties. Moreover, more pores may cause the Nd-rich phase to fill the pores and form aggregations, which can be observed in Fig. 6a, resulting in a low remanence and $(BH)_{max}$. The higher coercivity of this sample is mainly due to the small grain size.[19]

When the hot-pressing temperature increased to 550°C, a higher density and platelet grains with the largest length (shown in Table S-2 in the Supplementary material) can be guaranteed at the same time. From Fig. 6c and d, it can be seen that there are fewer stomata and aggregations of Nd-rich phases and that most of the grains have been transformed into lamellar grains, forming a better texture and resulting in higher remanence and
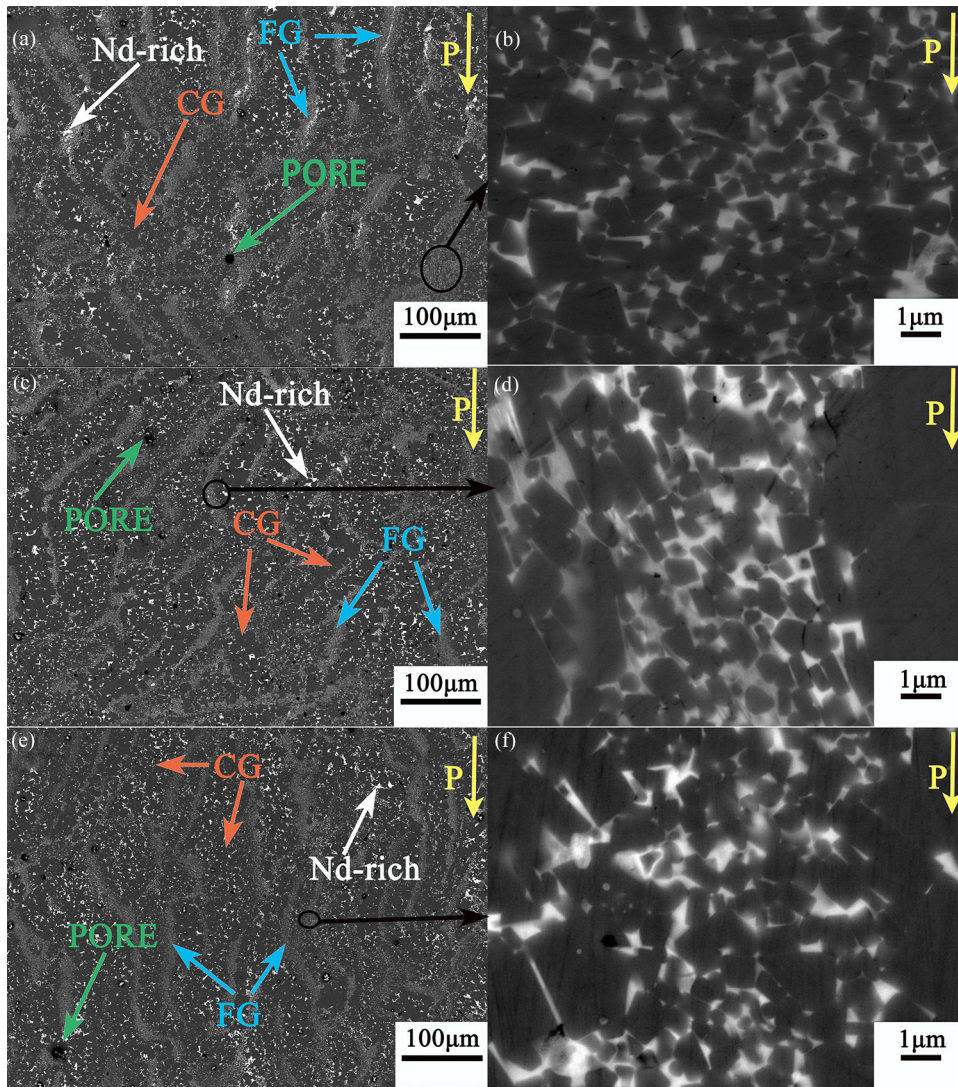
Fig. 6. Cross-section morphologies of the MM samples from the magnetic sheets hot-pressed at (a, b) 500°C, (c, d) 550°C, (e, f) 600°C and hot forward-extruded at 800°C with the deformation speed of 0.05 mm s^{-1}.

(BH)$_{max}$. When the hot-pressing temperature increased to 600°C, the grain width of the sample increased and its coercivity was the lowest.

The magnetic properties, demagnetization curves, and XRD patterns of the MM samples from the magnetic sheets hot-pressed at 550°C and hot forward-extruded at 800°C using different hot deformation rates are shown in Table II and Fig. 7. From Fig. 7a and Table II, it can be seen that the rectangularities of the demagnetization curves gradually deteriorates with the increase of the deformation speeds, and that the remanence and the maximum magnetic energy products also decrease. From Fig. 7b and Table II, it can be seen that the $I_{(006)}/I_{(105)}$ values of the MM samples hot-pressed at 550°C and hot forward-extruded at 800°C decreased from 1.09 to 0.57 when the hot deformation rates increased from 0.03 mm s^{-1} to

0.07 mm s^{-1}, indicating that the texture of the magnetic sheet became weakened with the increase of the hot-deformation rates.

Figure 8 shows the cross-section morphologies of the MM samples from the magnetic sheets hot-pressed at 550°C and hot forward-extruded at 800°C using different hot-deformation rates. From Fig. 8a, it can be seen that the sample using the hot-deformation rate of 0.03 mm s^{-1} has heterostructure layers parallel to the pressure direction and fewer pores than at the heat. From Fig. 8b, it can be seen that almost all the equiaxed grains have been transformed into flaky grains, elongated and arranged parallel to the pressure direction, indicating that this hot-deformation rate is very favorable for the formation and orientation of platelet grains. This is also the reason for its high residual magnetism and magnetic energy product.
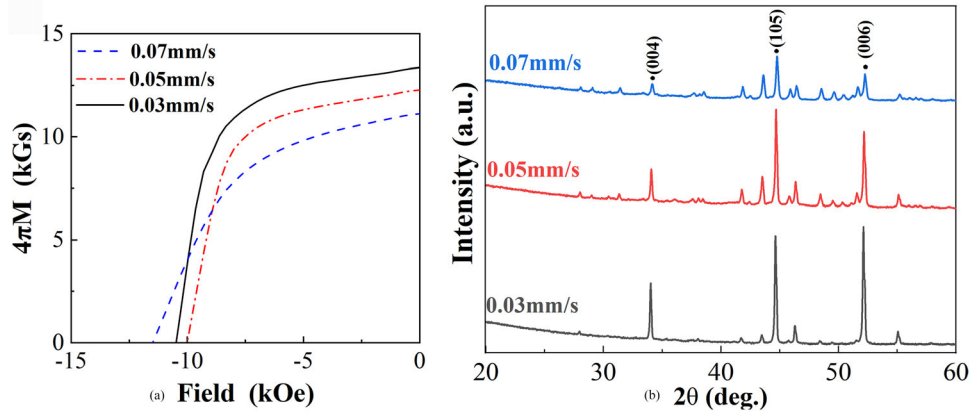
Fig. 7. Demagnetization curves (a) and XRD patterns (b) of the MM samples from magnetic sheets hot-pressed at 550°C and hot forward-extruded at 800°C using different hot-deformation rates.
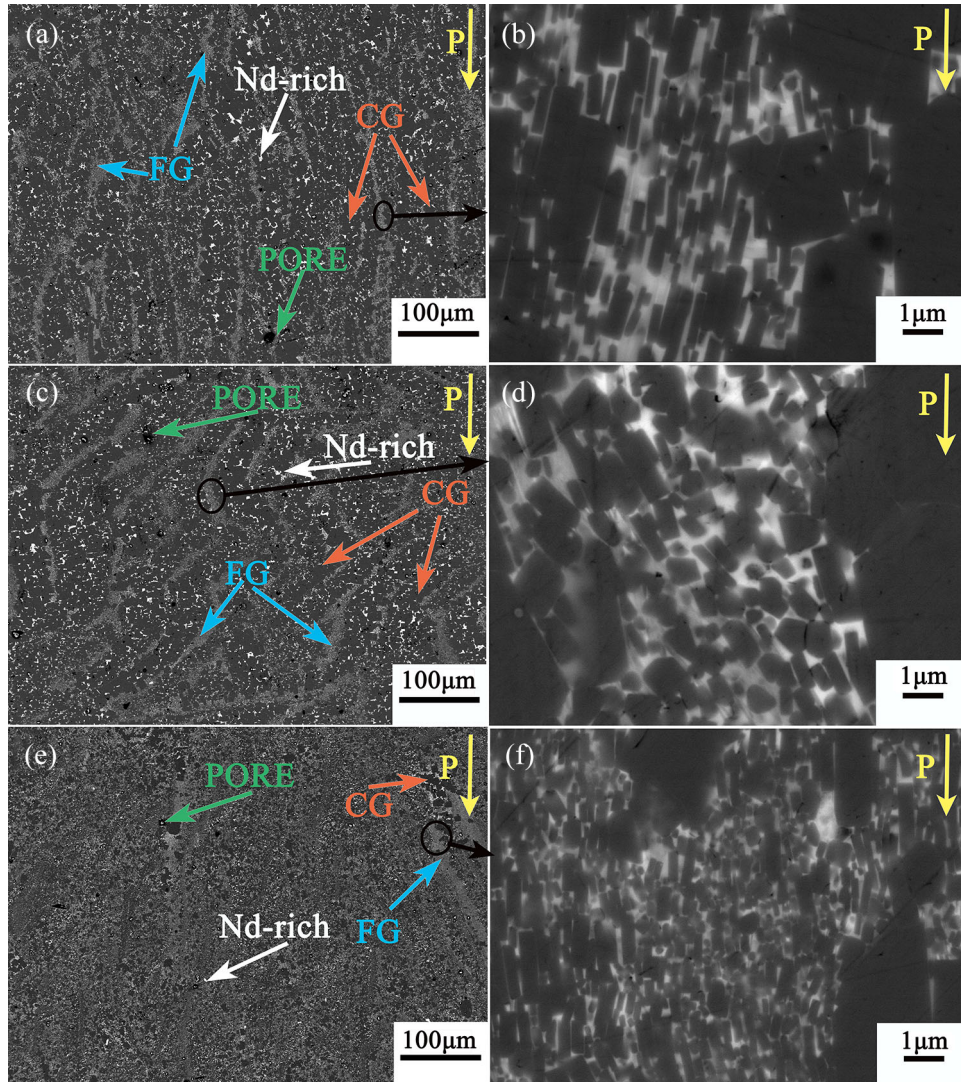

Fig. 8. Cross-section morphologies of the MM samples from the magnetic sheets hot-pressed at 550°C and hot forward-extruded at 800°C using hot deformation speeds of (a, b) 0.03 mm s^{-1}, (c, d) 0.05 mm s^{-1}, and (e, f) 0.07 mm s^{-1}.
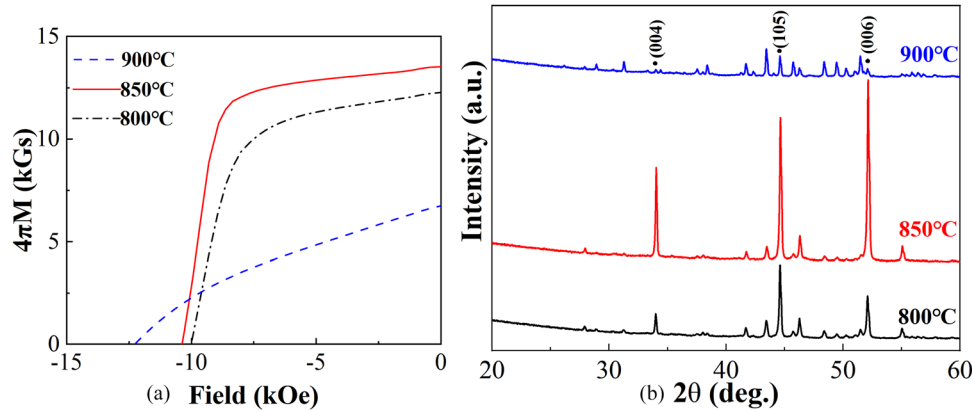
Fig. 9. (a) Demagnetization curves and (b) XRD patterns of the MM samples hot-pressed at 550°C and forward-extruded using the deformation speed of 0.05 mm s^{-1} at different temperatures.

When the hot-deformation rate reaches 0.05 mm s^{-1}, the heterostructure layers of the sample show an S shape along the pressure direction, and the fine pores increase (Fig. 8c). From Fig. 8d, it can be seen that the distribution of the lamellar grains has a certain angle to the pressure direction and becomes thicker and shorter than those grains of the sample using the hot-deformation rate of 0.03 mm s^{-1} (shown in Table S-3 in the Supplementary material), and that some equiaxed grains failed to deform into flake grains. As a result, the remanences and maximum magnetic energy products decreased. At this time, the grain size of the sample using the hot-deformation rate of 0.05 mm obviously increased compared with that of the sample using the hot-deformation rate of 0.03 mm s^{-1}, resulting in a decrease of coercivity.

When the speed increases to 0.07 mm s^{-1} (Fig. 8e), it can be seen that the structure of the sample using hot-deformation rate of 0.07 mm s^{-1} do not have obvious regular heterostructure layers, the coarse grain zone and fine grain zone are more messy, and the diffusion of atoms is inhibited due to the high hot-deformation rate.[20] From Fig. 8f, it is observed that most of the fine grains are spherical or short sheets, failing to grow and deform, and that the precipitation and orientation of the grains became difficult. Thus, the texture becomes weaker, and the remanence and the maximum magnetic energy product decrease. The excessively high deformation rate also results in the grains not being able to grow in time and the grain size is smaller, leading to the increase of the fine grain areas and the coercivities of the sample.

Figure 9 shows the demagnetization curves and XRD patterns of the MM samples hot-pressed at 550°C and forward-extruded using 0.05 mm s^{-1} at different temperatures. From Fig. 9a, we can see that the sample extruded at 850°C has the best rectangularity of the demagnetization curve. The sample extruded at 900°C has the worse rectangularity of demagnetization curve, and thus its

magnetic properties decrease greatly. From Fig. 9b and Table II, it can be seen that the $I_{(006)}/I_{(105)}$ of the sample forward–extruded at 800°C is 0.78, indicating the forming of an obvious texture. When the deformation temperature increased to 850°C, the $I_{(006)}/I_{(105)}$ of the sample increased to 1.28, indicating a strong texture. Further increasing the deformation temperature to 900°C, the $I_{(006)}/I_{(105)}$ of the sample dropped significantly to 0.32 and the texture became worse.

Figure 10 shows the cross-section morphologies of the MM samples hot-pressed at 550°C and forward-extruded using 0.05 mm s^{-1} at different temperatures. From Fig. 10, it can be seen that the grain size of the MM samples gradually increases with the deformation temperature (shown in Table S-4 in the Supplementary material). From Fig. 10a, it can be seen that the heterogeneous microstructure layers of the MM sample deformed at 800°C show an S-shape distribution and that there are more Nd-rich phase aggregations and pores. Most of the grains of the MM sample are transformed into platelets and their average length is 1.25 μm, while they show an angle to the pressure direction. This may be due to the lower deformation temperature weakening the fluidity of the Nd-rich phase, which limits the formation of lamellar grains and the grain orientation.

When the deformation temperature increased to 850°C, all the grains of the MM sample (Fig. 10b) are transformed into thin platelets with an average length of 1.50 μm parallel to the pressure direction. Its heterogeneous structure layer is distributed parallel to the pressure direction and there are very few pores. This is because the Nd-rich phase has good fluidity at higher temperature, which is conducive to the formation of the platelet grains and texture. The grain orientation is greatly improved, thus the maximum magnetic energy product and residual magnetism are very high. When the deformation temperature further increased to 900°C, the grains in the fine grain regions of the obtained
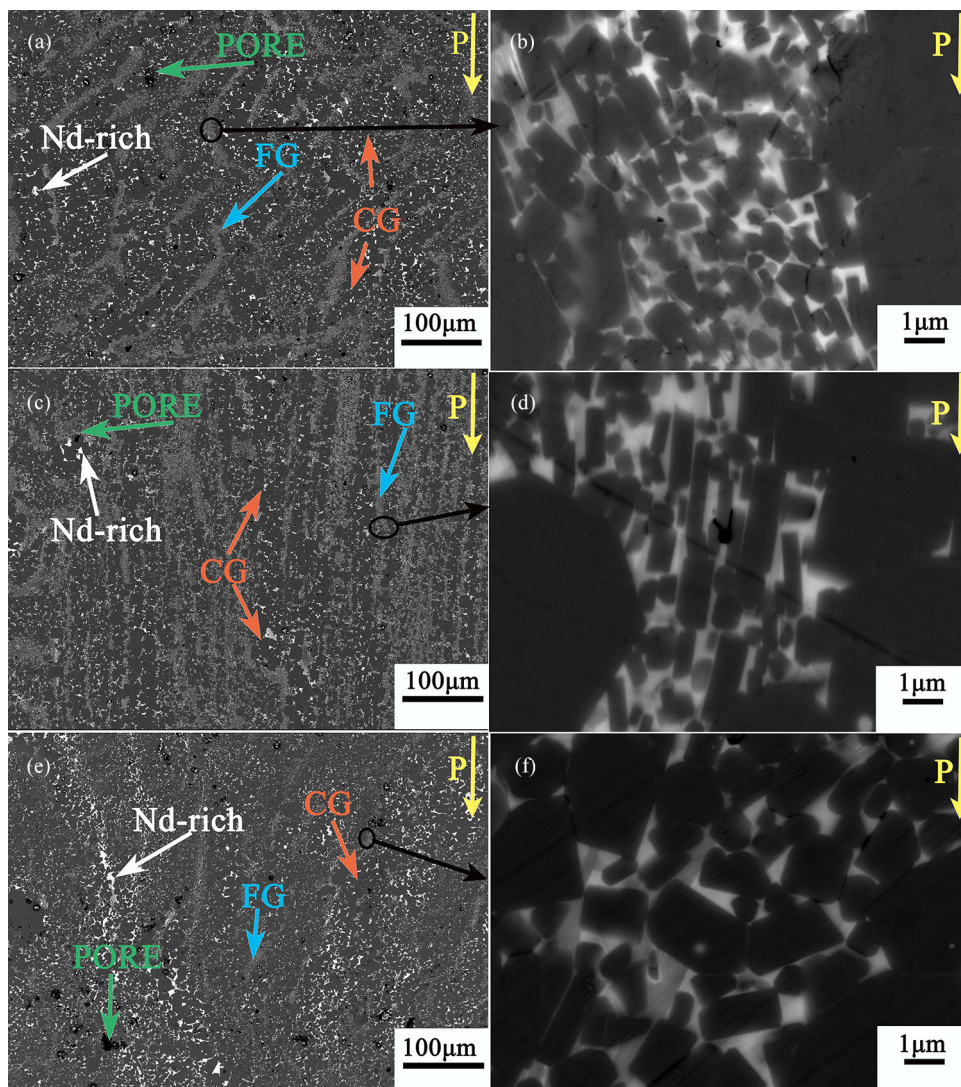
Fig. 10. The cross-section morphologies of the MM samples hot-pressed at 550°C and forward-extruded using deformation speed of 0.05 mm s^{-1} at (a, b) 800°C, (c, d) 850°C, and (e, f) 900°C.

sample were abnormally coarse. Coarse grains, which are difficult to be oriented, deformed and led to the loss of texture, which is the critical factor for such a dramatic decrease in remanence. The fluidity of the Nd-rich phase is excellent in such a high temperature and start to aggregate, leading to the emergence of a large number of pores, which also cause the low remanence and thus low maximum magnetic energy products.[21]

From Table I, we also find that the remanences increased with the increase of texture degree (shown in Figs. S-2, S-3, and S-4 in the Supplementary material). From Tables I and II, we can see that the highest coercivities are observed in the MT sample from the magnetic sheet hot-pressed at 550°C and forward-extruded at 800°C with the deformation speed of 0.05 mm s^{-1} (Table I) and the sample from the magnetic sheet hot-pressed at 550°C and forward-extruded at 900°C with the deformation speed of 0.05 mm s^{-1} (Table II) with

the least texture. As is known, the coercivity of hot-deformed Nd-Fe-B magnets has a strong correlation to the grain size. The smaller the grain size, the higher the coercivity of the magnet. However, from Tables S-1 and S-4 in the Supplementary material, we can see that the RT sample has a larger size than the RB, RM, or MM samples, and that the sample extruded at 900°C also has a larger size than the samples extruded at 800°C and 850°C. The reason maybe that the highest coercivities come from a strong domain wall pinning by the pinning sites at the nonmagnetic planar inhomogeneity boundaries between the platelet-shaped $Nd_2Fe_{14}B$ grains.[22]

CONCLUSION

Nd-Fe-B magnetic sheets have been fabricated using the hot forward-extrusion method and exhibit heterogeneous microstructure characteristics. With the decrease of extrusion speed, the $Nd_2Fe_{14}B$

grains become flat platelets with their *c*-axes parallel to the stress axis by grain rotating, and diffusion slip has been more fully completed, and the texture, remanence, and maximum magnetic energy product $(BH)_{max}$ of the forward-extruded magnetic sheet monotonically increased. With the increase of hot-pressing and deformation temperatures, the texture, remanence, and $(BH)_{max}$ of the hot-extruded magnetic sheet initially increased and then decreased. The grain size increased with the increase of the deformation temperatures, and, when the temperature was further increased to 900°C, the grains in the fine grain regions of the sample were abnormally coarse. Coarse grains, which are difficult to be oriented, deformed and led to the loss of texture, which is the critical factor for such a dramatic decrease in remanence.

SUPPLEMENTARY INFORMATION

ACKNOWLEDGEMENTS

CONFLICT OF INTEREST

The authors have no conflicts to declare.

REFERENCES

1. M. Sagawa, S. Fujimura, N. Togawa, H. Yamamoto, and Y. Matsuura, *J. Appl. Phys.* 55, 2083 (1984).
2. J.M.D. Coey, *Engineering* 6, 119 (2020).
3. Z. Jing, Z. Guo, M. Li, Y. He, X. Wang, M. Zhu, and W. Li, *J. Alloys Compd.* 792, 519 (2019).
4. O. Gutfleisch, M.A. Willar, E. Brück, C.H. Chen, S.G. Sankar, and J.P. Liu, *Adv. Mater.* 23, 821 (2011).
5. C. Song, Y. Wang, Y. Lü, and R. Wu, *Chin. Sci. Bull.* 65, 1251 (2020).
6. H. Tian, D.Z. Jin, Y. Li, M.Y. Zhu, and H.M. Jin, *J. Rare Earth* 24, 318 (2006).
7. X. Li, Q.Z. Jiang, S.U. Rehman, Q.F. Huang, Y.W. Chen, C.J. Zhao, and Z. Zhong, *J. Supercond. Nov. Magn.* 35, 251 (2022).
8. L. Zheng, K. Fang, L. Zhao, D. Zhou, R. Jiang, Z. Guo, M. Zhu, and W. Li, *JOM* 71, 3107 (2019).
9. T. Saito, M. Fujita, T. Kuji, K. Fukuoka, and Y. Syono, *J. Appl. Phys.* 83, 6390 (1998).
10. D. Hinz, A. Kirchner, D.N. Brown, B.M. Ma, and O. Gutfleisch, *J. Mater. Process. Technol.* 135, 358 (2003).
11. Y.Q. Li, Y.Y. Tang, W.Q. Liu, M. Yue, X.C. Xu, H.G. Zhang, and Q.M. Lu, *J. Magn. Magn. Mater.* 555, 169322 (2022).
12. Y. Li, X. Xu, M. Yue, D. Wu, W. Liu, and D. Zhang, *J. Rare Earth* 37, 1088 (2019).
13. Y. Tang, Y. Li, X. Xu, M. Yue, W. Liu, H. Zhang, and W. Xia, *J. Mater. Sci. Technol.* 80, 28 (2021).
14. K. Kojima, A. Ibata, and S. Kojima, *IEEE Transl. J. Magn. Jpn.* 4, 263 (1989).
15. Y. Li, S. Zuo, L. Zheng, M. Zhu, Y. Fang, L. Zhao, C. Li, W. Li, and G.C. Hadjipanayis, *J. Magn. Magn. Mater.* 577, 170781 (2023).
16. F. Wang, W. Shen, J. Fan, J. Du, K. Chen, and J.P. Liu, *Nanoscale* 11, 6062 (2019).
17. I. Dirba, S. Sawatzki, and O. Gutfleisch, *J. Alloys Compd.* 589, 301 (2014).
18. R.K. Mishra, *J. Appl. Phys.* 62, 967 (1987).
19. K. Xu, X. Liao, H. Yu, X. Zhong, Z. Liu, and G. Zhang, *J. Magn. Magn. Mater.* 537, 168193 (2021).
20. Y.-D. Kim, H.-R. Cha, J.-G. Lee, J.-H. Liu, and K. Shu, *IEEE Trans. Magn.* 51, 1 (2015).
21. J. Song, M. Yue, J. Zuo, Z. Zhang, W. Liu, D. Zhang, J. Zhang, Z. Zuo, and L. Wei, *J. Rare Earth* 31, 674 (2013).
22. F.E. Pinkerton and C.D. Fuerst, *J. Magn. Magn. Mater.* 89, 139 (1990).